ACTA TECHNICA JAURINENSIS
Vol. XX, No. Y, pp. ZZ-ZZ, 2025
10.14513/actatechjaur.00794

Research Article

Improving wear performance of Mg-4Zn alloy using Si_3N_4 nanoparticle reinforcements: Mass loss analysis

Anand Natarajan[1,2,*], Ramu Kumar Verma[3], Jayaprakash Reddy K[3], Bijulal D[2,4], Vijayan K[3], Prasanth Prabhakaran[3]
[1]Department of Mechanical Engineering, College of Engineering Trivandrum, Engineering College P.O, Sreekaryam, Thiruvananathapuram, Kerala, 695016, India
[2]APJ Abdul Kalam Technological University, Thiruvananathapuram, CET Campus, Thiruvananthapuram Kerala, 695016, India
[3]ISRO Inertial Systems Unit, Vattiyoorkavu PO, Thiruvananthapuram, Kerala, 695013, India
[4]Department of Mechanical Engineering, Government Engineering College Barton Hill, Kunnukuzhi, Thiruvananthapuram, Kerala, 695035, India
*e-mail: anandlight.win@gmail.com

Submitted: 20/05/2025 Revised: 25/07/2025 Accepted: 27/07/2025 Published online: 19/12/2025

Abstract: Si_3N_4 ceramic possesses superior wear properties and high-temperature properties. This research hypothesizes that very small quantities (0.23, 0.45, and 0.67 wt.%) of the biocompatible, bio-ceramic, Si_3N_4 nanoparticles (of 15-30 nanometre average particle size) added as reinforcements to the lightweight, biofriendly Mg-4Zn alloy matrix would improve the wear properties of the Mg-4Zn alloy. Hypothesis verification was done using design of experiments (DoE)-based dry sliding wear studies. Mg-4Zn alloy and Mg-4Zn/xSi_3N_4 (x=0.23, 0.45, and 0.67 wt.% nano-Si_3N_4) nanocomposites were the pin materials, and SS316Ti was used as the disc (counterface) material. Load and sliding speed were also varied. A regression model for predicting the mass loss was obtained using Design-Expert software. Worn surface analysis revealed that abrasion was the dominating mechanism of wear in all tested conditions. Adhesion wear was also observed at mild levels. The addition of 0.23, 0.45, and 0.67 wt.% nano-Si_3N_4 to Mg-4Zn alloy refined the grain size by 10.58, 34.32, and 63.94 %, respectively, thereby improving the microhardness by 8.11, 19.54, and 38.67 %, respectively, and reducing the mass loss up to 8.3%. The microstructural studies indicated α-Mg grains surrounded by Mg-Zn intermetallic at the grain boundaries.

Keywords: Mg-4Zn; Si_3N_4; wear; nanocomposites

I. INTRODUCTION

The development and production of lightweight materials is extremely important in the automotive and aviation industries [1] since their use is effective in improving fuel efficiency and reducing emissions [2]. Mg-based materials are a good choice as lightweight materials because of their low density of only 1.74 g/cm^3, higher specific stiffness, and specific strength [2]. They are also non-toxic and biodegradable [3] and also possess good impact resistance, damping capacity, and dimensional stability. They are also preferred for biomedical applications. In spite of many such advantages, low corrosion resistance and wear resistance are the disadvantages of Mg-based alloys [4]. Low wear resistance induces replacement of components with the passage of time [5]. To enhance the properties of Mg-based materials further, ceramic particles are used as reinforcements [4] to form Mg metal matrix composites (MMCs), which possess enhanced wear resistance, strength, high-temperature properties, and dimensional stability [6]. This is made possible by the activation of mechanisms such as the transfer of load to the reinforcements from the matrix, an increase in the density of dislocations near the matrix/reinforcement interface (caused by the difference in the coefficient of thermal expansion between the matrix and reinforcement), and grain refinement effects [7], [8]. The wear resistance of the AZ31 matrix was improved by nanoscale SiC_p of size 40-60 nm, which strengthened the AZ31 matrix due to grain refinement, as revealed by wear tests at 10 N, 20 N, and 30 N normal loads and 0.1, 0.3, and 0.5 m/s sliding speeds without lubricant using a GCr15 steel ball/pin pair [9]. The wear properties of heat-treated stir-cast AZ61 magnesium alloy were improved by the addition of CNTs (concentration of

0, 0.1, 0.5, and 1 wt.%) as reinforcements [10]. Reinforcements like TiO_2, Mg_2Si, SiC, Al_2O_3, Y_2O_3, TiC, and TiB_2 have also been used [11] for property improvements. Among various Mg-based materials, the Mg-4Zn alloy (Mg alloyed with 4 wt.% Zn) possesses good biocompatibility, a low rate of degradation, and moderate mechanical properties [12], [13], [14]. This alloy is represented in the Mg-Zn phase diagram as shown in **Fig. 1.**

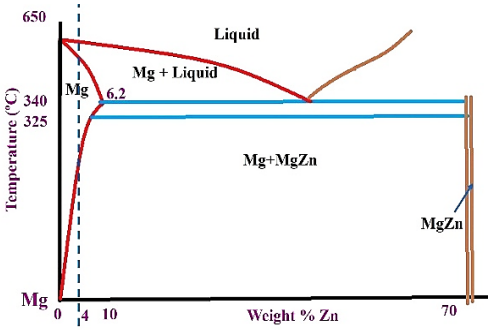

Figure 1. *Mg-4Zn alloy in Mg-Zn phase diagram [15]*

Some attempts to improve its properties further, like the solution treatment to improve its corrosion resistance [16] and multi-directional forging to improve the microhardness and wear resistance [17], have been reported in the literature. The Mg-4Zn alloy offers scope for further improvement in its wear properties by the use of Si_3N_4 in the form of nanoparticle reinforcements, which has not been explored to the best knowledge of the authors. Nanoparticles can effectively influence the hardness [18] and hence wear properties [19]. The addition of 0.22 to 1.11 vol. % Al_2O_3 of 50 nm particle size improved the wear resistance of pure Mg (direct metal deposited), as revealed by wear tests conducted at 10 N at 1 to 10 m/s sliding speed [20]. The addition of 0.5-2 wt.% CNT with 20-40 nm size improved the wear resistance of AZ91D by 16.99% (AZ91D-2CNT). A load of 4–12 N and a sliding speed of 0.1 to 0.2 m/s revealed the wear resistance improvement [21]. Silicon nitride (Si_3N_4) is a material that has very good wear resistance, mechanical properties, and thermal stability. It is used in roller and ball bearings and in rotors [22]. It has also been used as nanoparticles to reinforce the AZ81 alloy [23] and in the form of whiskers as reinforcements to improve the hardness (Vickers), ultimate compression strength (UCS), and properties of pure Mg [24].

This research attempts to improve the wear properties of Mg-4Zn alloy by using Si_3N_4 in the form of nanoparticles of 15-30 nm average particle size as reinforcements in the Mg-4Zn alloy and presents the regression model for the mass loss. It is hypothesized in this research that the Si_3N_4 particles used in the nanoscale would contribute to grain refinement, improve the hardness, and hence improve the wear properties of the Mg-4Zn alloy. This is represented as a schematic in **Fig. 2**. However, it is also reported that nearly 1 wt.% of nano-reinforcement additions could adversely affect the properties due to the effects of agglomeration [25]. Therefore, very low proportions (0.23, 0.45, and 0.67 wt.%) of Si_3N_4 were chosen to enhance sustainable production and effective material utilization of Mg-4Zn/Si_3N_4 nanocomposites and to avoid agglomeration.

Figure 2. *Using Si_3N_4 nanoparticles to improve wear properties of Mg-4Zn alloy*

To validate this hypothesis, initially, trial (pilot) studies were done by the authors to ensure that the material combination possessed reasonable properties. This research presents the systematic experimental studies that were then conducted to validate the hypothesis and obtain a regression model for mass loss. This research becomes more significant since Si_3N_4 (used to reinforce Mg-4Zn alloy) is also a bio-ceramic, is biocompatible (like Mg alloys), and has good application potential [26]. The use of large quantities of Al and rare earth additions to Mg is avoided [27]. Moreover, quantitative outcomes of this research could promote economical, efficient production of Mg-4Zn alloy and diversify its applications. Stir casting is a commercially practiced manufacturing method that is flexible, simple, and can be used for mass production of composite products [28]. Therefore, vacuum stir casting has been used for the production of the base alloy and nanocomposites. Pin-on-disc studies with the Mg-4Zn-based materials as pins and SS316Ti stainless steel as disc is presented. SS316 stainless steel is also a material of interest for wear studies. Fellah et al. [29] studied the tribological characteristics of AISI316L stainless steel under a normal load of 3 N, 6 N, and 10 N and a sliding speed of 1, 15, and 25 mm/s. Parthasarathi et al. [30] performed wear tests on AISI316L stainless steel at different temperatures up to 550°C at 20 N load and a 0.8 m/s sliding speed with the pin-on-disc arrangement.

II. MATERIALS AND METHODS

Vacuum stir casting was carried out in a SWAMEQUIP-made stir casting furnace with a bottom pouring arrangement to produce cylindrical rods of the Mg-4Zn alloy and Mg-4Zn/Si_3N_4 nanocomposites. **Fig. 3** illustrates the schematic of

the process of the vacuum stir casting and the arrangement for wear testing. After cleaning the inner surface of the furnace, a graphite-based non-stick coating was applied. A temperature of 750°C was achieved in the furnace. High-purity gas (argon: SF6 = 9:1) was used in the furnace for shielding. Mg and Zn as ingots were melted in the furnace to form the Mg-4Zn alloy melt. It was continuously stirred at 500 rpm. Si_3N_4 nanoparticles (made by Nanoshel UK Limited) having a purity of 99% and 15-30 nm average particle size (APS) were first preheated to 200°C for 45 minutes to avoid thermal shock and remove moisture. The nanoparticles were added to the melt in the required proportions (wt.%) by wrapping them in an Al foil. Ultrasonic vibration (20 kHz, 3-5 min) was used to prevent agglomeration. The composite was stirred for 10 minutes at a temperature of 750°C to ensure that the constituents were distributed homogeneously and poured into a cylindrical mold of 250 mm length and 30 mm diameter, vacuum pressure of 1 bar was applied. The mold with the molten alloy/nanocomposite was cooled to room temperature under normal atmospheric conditions. After the casting solidified, it was removed from the mold. To produce the Mg-4Zn alloy, the above procedure was followed except for the addition of Si_3N_4 nanoparticles.

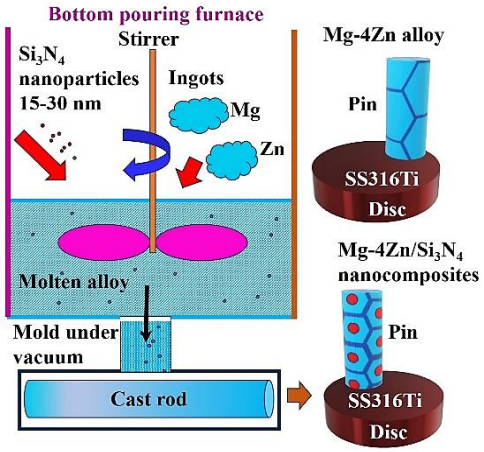

Figure 3. *Schematic illustration of vacuum stir casting and pin-on-disc arrangement for wear testing*

2.1 Evaluation of material properties

Specimens were obtained from the castings for the material characterization and wear studies (**Fig. 3)**, respectively. The specimens for the X-ray studies were prepared by polishing with rough and fine emery sheets, followed by polishing with alumina powder and diamond paste (0.5 to 1 µm size). The polished surfaces were studied by X-ray diffraction using a 20-minute scan of angles from 5 to 100 degrees in a Rigaku SmartLab X-ray diffractometer and subjected to wavelength dispersive X-ray fluorescence spectroscopy (XRF) studies in a Bruker S8 Tiger Series II 4 kW WDXRF machine. The specimens for optical and scanning electron microscopic (SEM) studies were prepared by polishing with emery sheets and alumina powder and then etched using acetic picral, which was obtained by mixing 10 ml acetic acid, 10 ml water, 70 ml ethanol, and 4.2 g picric acid. These were then observed under a Dewinter optical microscope, from which optical micrographs were obtained. The average grain size of 50 grains of each material was calculated manually from the optical micrographs by using ImageJ software. SEM images were obtained from the ZEISS SEM with Energy Dispersive Spectroscopy (EDS) and elemental mapping facilities after ultrasonication of the specimens in isopropyl alcohol solution. Microhardness tests of these specimens were done using FIE equipment at a 500 g load and a dwell time of 15 seconds. The average of five measurements is considered. The specimens were weighed by employing a Mettler Toledo electronic weighing machine, which is capable of measuring from ± 0.0001 g. The density (ρ_{Actual}) of the materials was calculated in accordance with Archimedes' principle as in Eqn. (1).

$$\rho_{\text{Specimen in air}} = \left(\frac{W_{\text{in air}}}{W_{\text{in air}} - W_{\text{in water}}}\right) \rho_{\text{water}} \quad (1)$$

where ρ indicates density and w indicates the weight of the material. The porosity was calculated according to Eqn. (2).

$$\text{Porosity (\%)} = \left(1 - \frac{\rho_{\text{Actual}}}{\rho_{\text{Theoretical}}}\right) \times 100 \quad (2)$$

2.2 Wear Testing

Mg-4Zn alloy and Mg-4Zn/Si3N4 nanocomposites were the pin materials, and SS316Ti was the disc material, as shown in Fig. 3. Pin-shaped specimens with a diameter of 10 mm and a height of 13 mm were machined from the vacuum stir cast Mg-4Zn alloy and Mg-4Zn/Si3N4 nanocomposites by using the wire electric discharge machining (EDM) process for the wear testing. Fig. 4 shows the test setup and the test specimens (inset). The surfaces of the pins were then thoroughly polished, first sequentially by emery sheets and then by diamond paste (0.5 to 1 µm size).

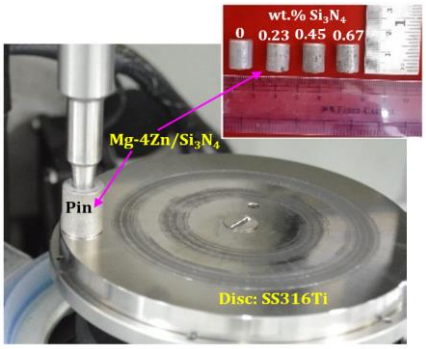

Figure 4. *Test setup for the wear experiments and wear test specimens (inset)*

It was ensured that the surfaces of the pins and disc had good surface flatness, parallelism and surface finish. The disc material was annealed SS316Ti stainless steel with 149 BHN. It was first machined to 90 mm in diameter and 7 mm in thickness by a facing operation. This was followed by surface grinding. They were then thoroughly polished, first by using alumina powder followed by diamond paste (0.5 to 1 µm size) to ensure a good quality surface with proper surface finish. The ASTM G99-17 standard was used as a guideline for the specimen preparation. An experimental design matrix (Taguchi L8) was obtained from software for the range of input process parameters as shown in Table 1. In addition to Si3N4 wt.%, load and sliding speed were also varied.

Table 1 *Input process parameters, their range and responses of the wear test*

nano-Si_3N_4 (wt.%)	***Load (N)***	***Sliding speed (m/s)***	***Responses***
0 0.23 0.45 0.67	4 8	0.85 1.1	Mass Loss (g) CoF

All tests were conducted with 510 m as the sliding distance in the pin-on-disc arrangement using a CETR tribometer. The randomized tests were performed at 22°C at a relative humidity of 50% and under dry sliding conditions. The pins and disc were cleaned with alcohol and dried before and after testing. The forces were measured using a load cell, and the coefficient of friction (CoF) was also recorded. The mass of the specimens before and after the wear test was measured by a Mettler Toledo electronic weighing balance with an accuracy of ±0.0001 g. Mass loss was calculated as the difference in weight of specimens before and after the wear test. The average value of three trials of the responses for each test condition is reported. A regression equation and a significant model were obtained for mass loss using Design-Expert software, using which the statistical analyses of the model were also performed. ANOVA analysis was performed, and R2, adjusted R2, and predicted R2 were obtained using the software. The worn surfaces were analyzed by SEM to identify the wear mechanism. OriginLab software was used for plotting graphs. The COF is calculated as the ratio of the friction force to the normal load [31].

III. Results and Discussion

The results obtained from the characterization and wear studies of the Mg-4Zn alloy and Mg-4Zn nanocomposites are presented.

3.1 Nanocomposite properties

The densities and porosities of the materials are shown in Table 2 which also shows the wt.% of Mg and Zn confirmed by XRF. Fig. 5 shows the scanned area, and Fig. 6 shows the SEM elemental maps in the scanned area of the Mg-4Zn-base alloy and nanocomposites. Low values of porosities in all the castings indicate good quality of the castings. The density of the base alloy (Mg-4Zn) is 1.773 g/cc. The densities of the Mg-4Zn nanocomposites with 0.23, 0.45, and 0.67 wt.% Si3N4 are 1.753, 1.737, and 1.769 g/cc, respectively. The density slightly decreases as the wt.% of Si3N4 increases from 0 to 0.45 wt.%.

Table 2 *Density, porosity, and Mg, Zn quantified by XRF*

wt. % Si_3N_4	***Density (g/cc)***	***Porosity (%)***	***Mg (wt.%) (XRF)***	***Zn (wt.%) (XRF)***
0	1.773	0.93	96	3.49
0.23	1.753 (-0.02)	2.18 (+1.25)	95.8	3.56
0.45	1.737 (-0.016)	3.26 (+1.08)	94	3.86
0.67	1.769 (+0.032)	1.55 (-1.71)	94.5	3.66

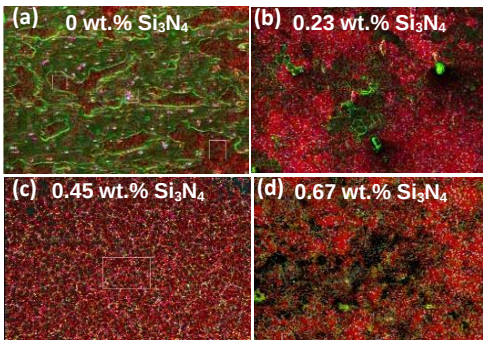

Figure 5. *Scanned area of the SEM elemental maps of Mg-4Zn base alloy and nanocomposites*

Correspondingly, the porosity has increased from 0.93 to 3.26 % respectively, thereby decreasing the density. The addition of the Si3N4 nanoparticles and stirring increases the viscosity of the melt. The air/gas bubbles get entrapped and are unable to escape the melt because of the higher viscosity, as observed by Aravindan et al. [32]. This leads to the entrapment of air/gas, leading to porosity in the stir castings. The density of Mg-4Zn nanocomposite with 0.67 wt.% Si3N4 is higher than the other nanocomposites and the base alloy. This could be due to the predominating effect of better wetting of Si3N4 reinforcement particles by the matrix alloy, which decreased the porosity and hence increased the density, as observed by Tosun et al. [33]. The SEM elemental maps (Fig. 6) are indicative of a homogeneous distribution of the elements Mg, Zn, Si, and N, thereby ensuring homogeneous

distribution of alloy and the Si3N4 reinforcement in the vacuum stir castings.

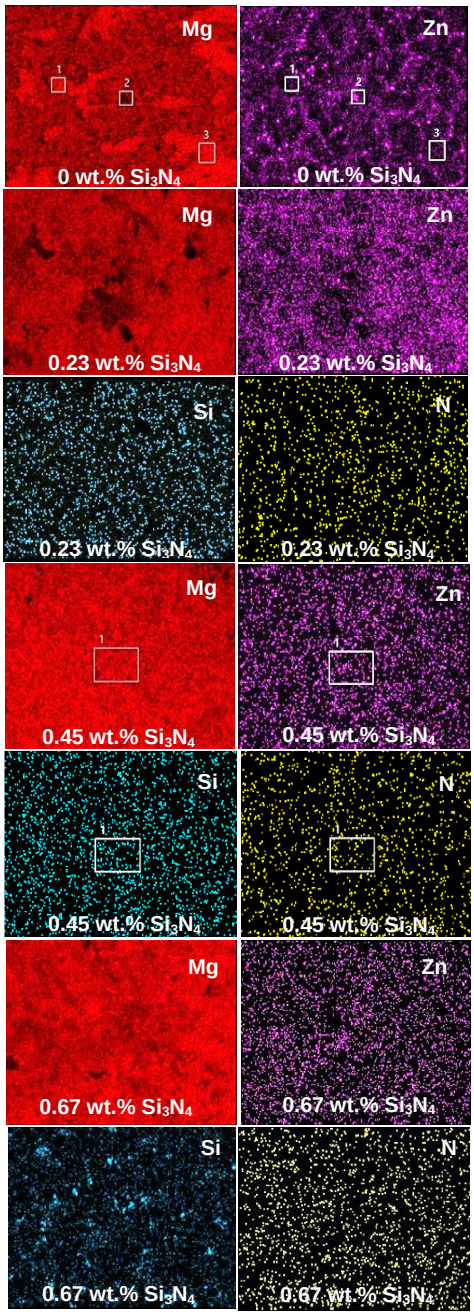

Figure 6. *SEM elemental maps of Mg-4Zn base alloy and nanocomposites*

The Mg and Zn wt.% in the base alloy and nanocomposites confirmed by X-ray fluorescence spectroscopy are shown in Table 2, thus quantifying the amount and proportion of Mg and Zn in all the materials. Fig. 7 presents the XRD plots of the materials, Peaks corresponding to α-Mg and Mg-Zn intermetallic were confirmed in the XRD plots of the base alloy and nanocomposites. This agrees with the expected microstructures obtained upon cooling the Mg-4Zn alloy as shown in the Mg-Zn phase diagram (Fig. 1). This justifies the formation of α−Mg grains, accompanied by intermetallic (Mg-Zn) segregating at the boundaries of grains in the base alloy and the nanocomposites. This is also consistent with the results reported by Wang et al. [34]. The small additional peak (of Si_3N_4) at 44° [35] for the Mg-4Zn nanocomposite with 0.45 wt.% Si_3N_4 in the XRD plot is attributed to the possible local agglomeration of Si_3N_4 particles at the location. The optical micrographs (**Fig. 8**) of the Mg-4Zn based materials show equiaxed α−Mg grains in the base alloy and the nanocomposites. Progressive grain refinement has occurred by the addition of Si_3N_4 reinforcement nanoparticles. **Table 3** quantifies the grain size reduction and microhardness improvement. **Fig. 9(a)** and **Fig. 9(b)** are schematics of the variation of grain size and microhardness, respectively, with Si_3N_4 wt.%. The average values of grain sizes of 50 grains were 207.5 (≈208), 185.8 (≈186), 135.8 (≈136), and 74.5 (≈75) µm for the base alloy and nanocomposites with 0.23, 0.45, and 0.67 wt.% additions of Si3N4 respectively.

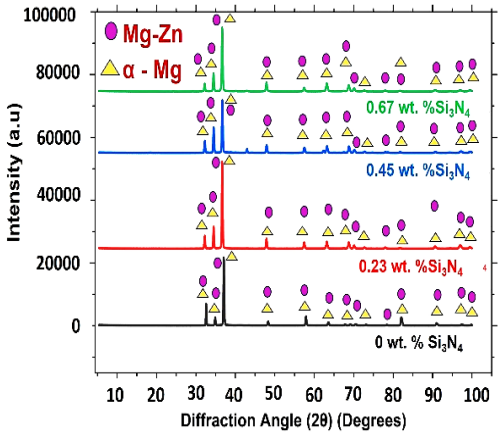

Figure 7. *XRD plots of the Mg-4Zn-based materials*

Table 3 *Grain size reduction and microhardness improvement percentages*

wt.% Si_3N_4	*Grain Size (µm)*	*Grain refinement (%)*	*Microhardness (HV0.5)*	*Microhardness Improvement (%)*
0	208	-	48	-
0.23	186	10.58	52	8.11
0.45	136	34.62	58	19.54
0.67	75	63.94	67	38.67

The average grain size decreased by 10.6 %, 34.62 %, and 63.94 % with the additions of 0.23, 0.45, and 0.67 wt.% Si3N4 to Mg-4Zn. The reduction in grain size by the Si3N4 additions is attributed to the increased heterogeneous nucleation caused by the Si3N4 nanoparticles, which increases with the number of Si3N4 nanoparticles [36]. The Vickers microhardness of the Mg-4Zn alloy is 48 HV0.5, and

that of the nanocomposites with 0.23, 0.45, and 0.67 wt.% Si3N4 are 52, 58, and 67 HV0.5, respectively, which indicates an increase of microhardness by 8.11, 19.54, and 38.67%, respectively.

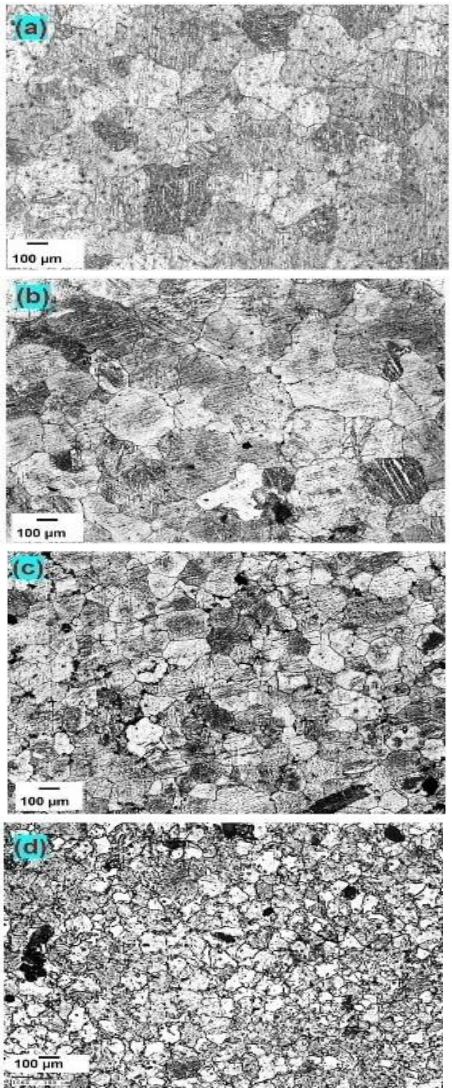

Figure 8. *Optical micrographs of the (a) Mg-4Zn alloy and Mg-4Zn nanocomposites with (b) 0.23, (c) 0.45 and (d) 0.67 wt.% Si_3N_4*

This could be due to the hard Si3N4 particles, which impede the dislocation movement and increase the resistance to deformation and consequently increase the hardness of the nanocomposites [37] as elaborated in **Fig. 9**. The Si_3N_4 particles promote heterogeneous nucleation within the Mg grains and inhibit the growth of grains (resulting in lesser grain size) [36]. Lesser grain size implies more grain boundaries, which prevent the movement of dislocations. The Si_3N_4 nanoparticles, which are dispersed throughout the matrix, can also pin the dislocations and restrict their movement. When an external stress is applied, the deformation resistance increases, and hence the strength increases. This is according to the Hall-Petch relation [38], [19], which substantiates an increase in strength with a decrease in grain size, as shown in **Fig. 9**. Orowan strengthening and load transfer effects brought about by the addition of Si_3N_4 nanoparticles could have also caused the microhardness improvement. An improvement in hardness also shows that there is good interfacial bonding [7] in the materials. The improvement in hardness (observed upon indentation) occurs due to the constraining of the local deformation of the matrix [39]. The strength increase with reduction of grain size could be attributed to the Hall-Petch relation [19]. The increase in hardness is also attributed to the increase in strength [40].

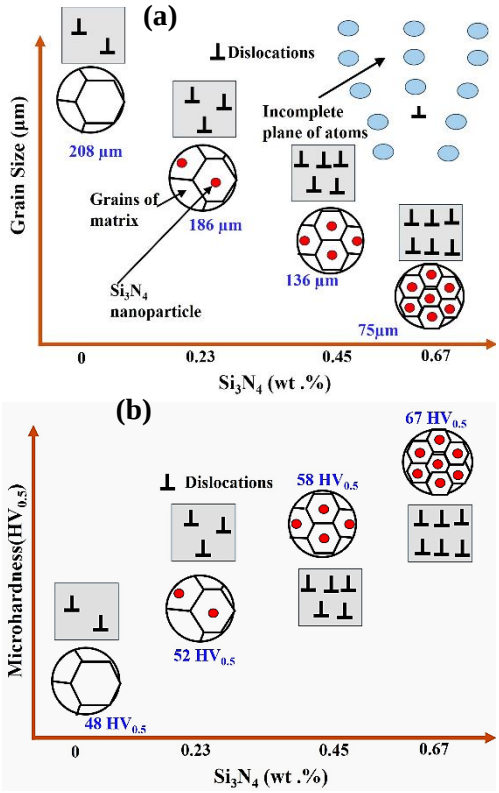

Figure 9. *(a) Grain size reduction and the (b) consequent improvement in microhardness by the addition of Si_3N_4 nanoparticles to Mg-4Zn alloy*

3.2 Wear properties

Table 4 shows the average mass loss and CoF obtained from the wear experiments for the various conditions tested. *ANOVA* analysis of the model for mass loss using the results of the wear experiments yielded an *F-value* of 24.90, which affirms the significance of the model. There is only a 0.48% chance that an *F-value* could have been caused by the noise. The R^2, adjusted R^2, and predicted R^2 values of the model are 0.9492, 0.9111, and 0.7716, respectively. The predicted R^2 is in reasonable agreement with the adjusted R^2, since they differ by less than 0.2 which qualifies the model to be used for prediction [41]. *Adeq Precision* quantifies the signal-to-noise ratio. *Adeq Precision* of 9.411 (greater than 4) indicates a signal that is adequate, making this model good to be used for traversing the design

space. The regression equation of mass loss is obtained (Eqn. (3)), where *A* is wt.% Si_3N_4, *B* is load, and *C* is sliding speed. To study the sensitivity of the mass loss to the Si_3N_4 wt.%, load, and speed, a perturbation plot is studied. It shows the changes in the response when each factor is moved from the reference point when all other factors are held at the reference value. The steeper the slope or the more the curvature, the more sensitive the response is to the factor. **Fig. 10** shows the perturbation plot of the mass loss. It is evident that mass loss is more sensitive to load (*B*) than to sliding speed (*C*) and the Si_3N_4 wt.% (*A*). It is evident that the mass loss decreases as the Si_3N_4 wt.% increases and the mass loss increases steeply with load and slightly with sliding speed. **Fig. 11** shows the plot of predicted and experimental values of mass loss.

Table 4 *Experimental design matrix and the corresponding values of the mass loss and CoF*

Si_3N_4 (wt.%)	***Load (N)***	***Sliding Speed (m/s)***	***Mass Loss (g)***	***CoF***	***Run Order***
0	4	0.85	0.0098	0.23	1
0	8	1.1	0.0161	0.22	5
0.23	4	0.85	0.0072	0.23	2
0.23	8	1.1	0.0171	0.21	6
0.45	4	1.1	0.0086	0.23	7
0.45	8	0.85	0.0145	0.22	3
0.67	4	1.1	0.0081	0.23	8
0.67	8	0.85	0.0166	0.22	4

It is evident that the experimental and predicted values do not differ by a large number, thus validating the goodness of the model. Fig. 12 is constructed from the regression equation for mass loss, Eqn. (3), which is obtained from the wear experiments.

$$Mass\ Loss\ (g) = -0.000540 - 0.001063A + 0.001909B + 0.001740C \quad (3)$$

It shows the percentage reduction in mass loss, which is indicative of the wear properties of the material for various weight percentages of Si3N4. A material with low mass loss has better resistance to wear. It is evident that for all tested conditions, the reduction in the mass loss increases with wt.% Si3N4. Lower mass loss and hence lower wear is attributed to the increased hardness (and hence higher deformation resistance) of the nanocomposites caused by the Si3N4 reinforcements. This could have made it difficult for the disc material to remove material (mass) from the pins, i.e., wear. This could be substantiated by Archard's law, which states that the wear rate decreases with an increase in hardness [19]. The highest reduction in mass loss is for 0.67 wt.% Si3N4. This shows that the nanocomposite with 0.67 wt.% Si3N4 has the best wear properties of the materials chosen for the testing. The possible dislodging of wear-resistant Si3N4 reinforcement particles [22] from the matrix and their presence at the interface of the pin and disc during the wear test also could have decreased the wear [42] [43].

Fig. 13 and **Fig. 14** show the worn surfaces for each test condition at 0.85 and 1.1 m/s, respectively. For all the test conditions, large parallel grooves oriented in the direction of sliding are observed. These are suggestive of plastic deformation due to abrasive wear operating as the predominant wear mechanism in the base alloy and nanocomposites [5]. Parallel grooves indicate abrasive wear [39]. This could be due to two-body abrasion in which the abrading particles are mounted on the abrading surface and rub over the soft surface acting similar to a tool [44]. **Fig. 15** and **Fig. 16** show the SEM EDS analysis of the worn surfaces tested at 0.85 and 1.1 m/s, respectively. There were no peaks beyond the region of EDS presented in **Fig. 15** and **Fig. 16**. Mg and Zn from the matrix were detected for all tested conditions of the Mg-4Zn base alloy and nanocomposites. At 0.85 m/s, the Mg-4Zn base alloy (**Fig. 15 (a)**) and the nanocomposite with 0.67 wt. Si_3N_4 (**Fig. 15 (d)**) additionally show adhesive wear which is confirmed by the presence of small quantities of *Fe* on the pin surfaces. *Fe* could have been transferred to the pin surface from the SS316Ti disc (which was the only possible source of *Fe* in the wear test system) due to adhesion [45]. However, *Fe* was not detected on the worn surfaces of pins tested under other conditions, probably due to its presence in amounts lower than the detectable level by the SEM EDS detector. The elevated levels of oxygen (*O*) were also identified on the worn surfaces of pins. These are attributed to the possible formation of an oxide layer since magnesium-based materials are highly oxidizable and/or due to the high temperatures generated at the unlubricated pin/disc interface during the wear test [46].

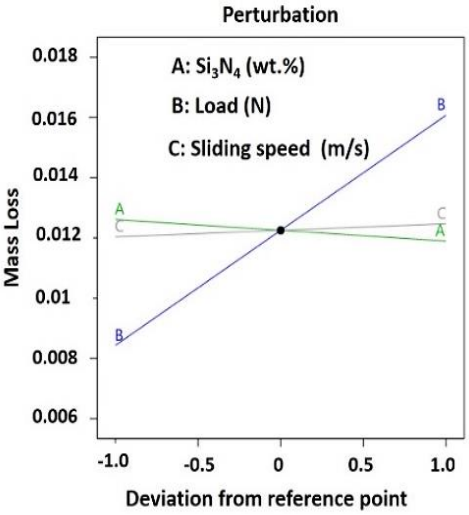

Figure 10. *Perturbation plot of the mass loss*

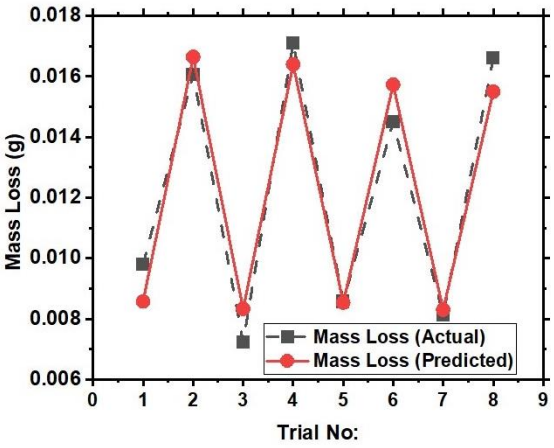

Figure 11. *Plot of experimental and predicted values of the mass loss*

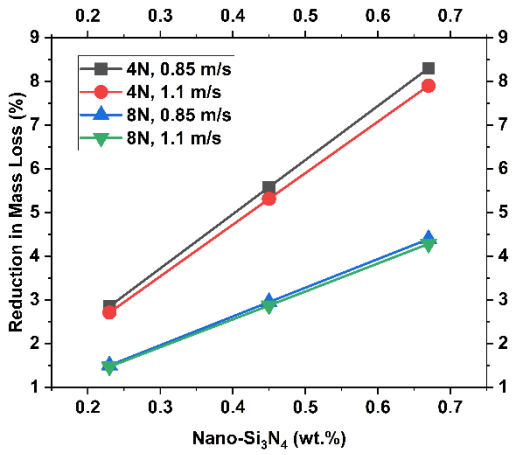

Figure 12. *Reduction in Mass Loss % vs. wt.% Nano-Si_3N_4*

(a) 0 wt.% Si_3N_4, 4N

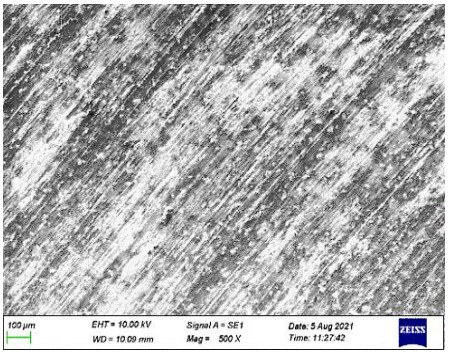

(b) 0.23 wt.% Si_3N_4 4N

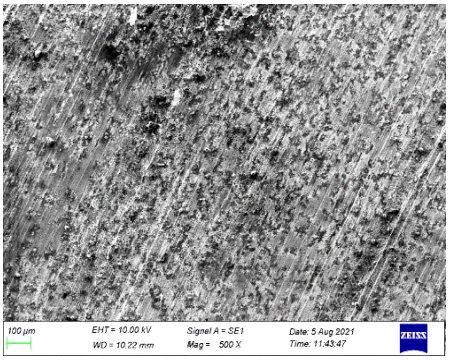

(c) 0.45 wt.% Si_3N_4, 8N

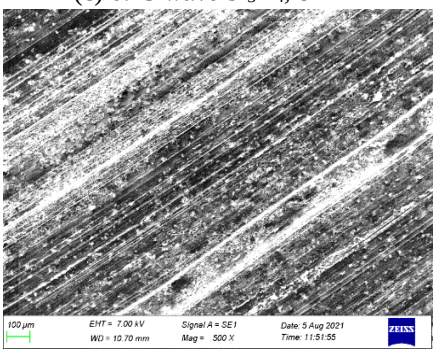

(d) 0.67 wt.% Si_3N_4, 8N

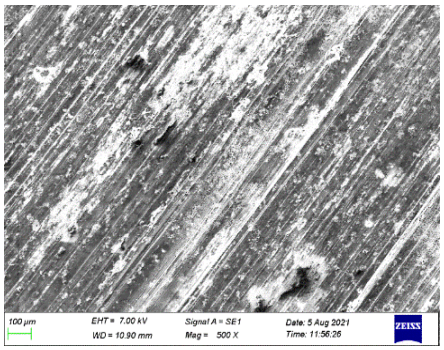

Figure 13. *Worn surfaces of specimens tested at 0.85 m/s*

(a) 0 wt.% Si_3N_4, 8N

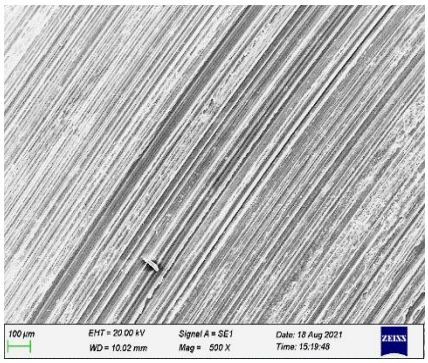

(b) 0.23 wt.% Si_3N_4, 8N

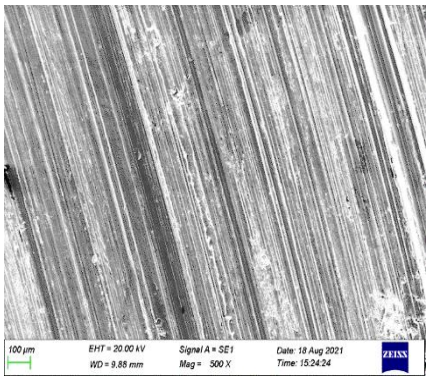

(c) 0.45 wt.% Si_3N_4, 4N

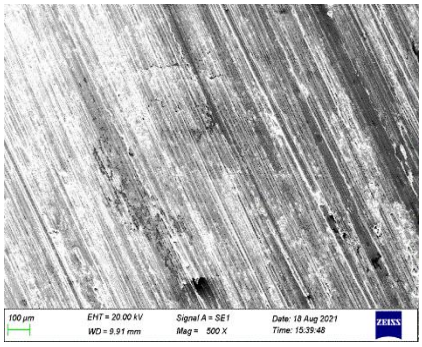

(d) 0.67 wt.% Si_3N_4, 4N

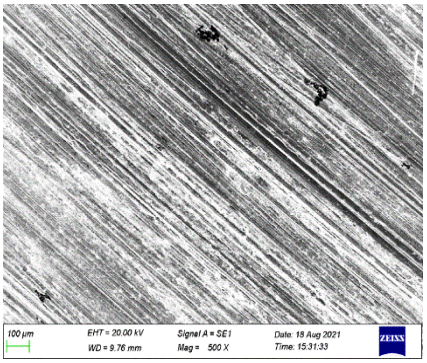

Figure 14. *Worn surfaces of specimens tested at 1.1 m/s*

(a) 0 wt.% Si_3N_4, 4N

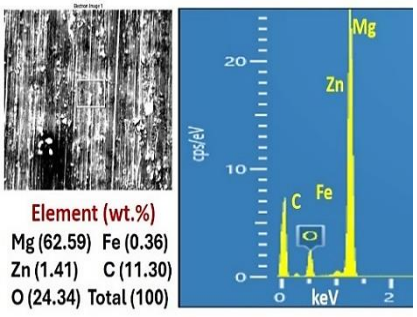

(b) 0.23 wt.% Si_3N_4, 4N

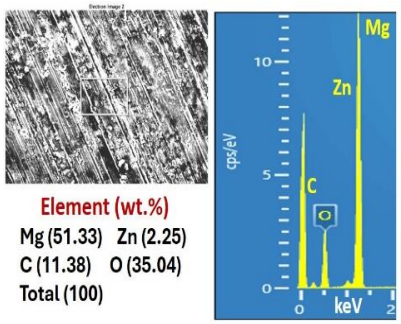

(c) 0.45 wt.% Si_3N_4, 8N

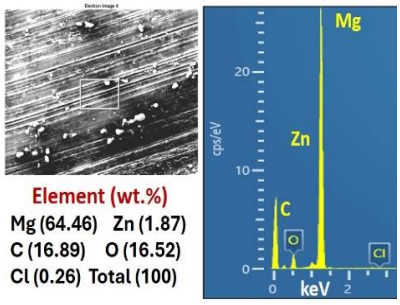

(d) 0.67 wt.% Si_3N_4, 8N

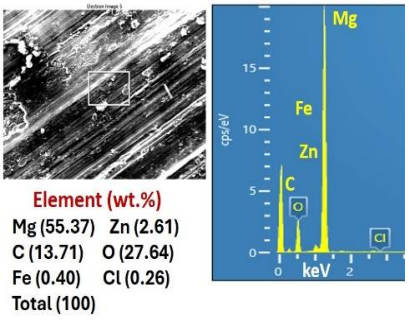

Figure 15. *SEM EDS analysis of worn surfaces of specimens tested at 0.85 m/s*

(a) 0 wt.% Si_3N_4, 8N

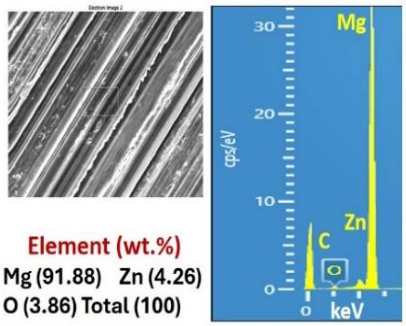

(b) 0.23 wt.% Si_3N_4, 8N

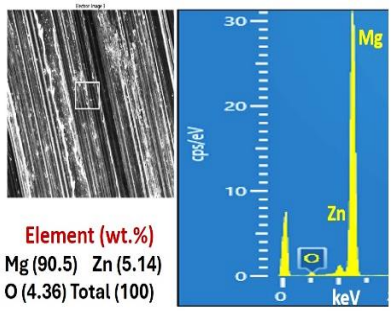

(c) 0.45 wt.% Si_3N_4, 4N

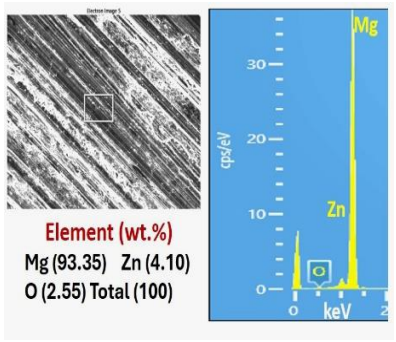

(d) 0.67 wt.% Si_3N_4, 4N

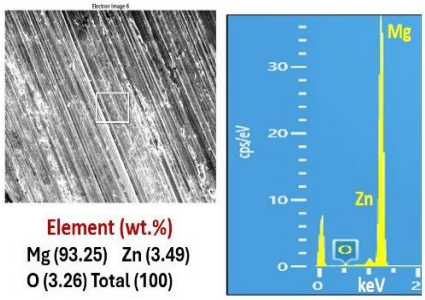

Figure 16. *SEM EDS analysis of worn surfaces of specimens tested at 1.1 m/s*

IV. CONCLUSIONS

From the wear tests conducted on Mg-4Zn-based materials with 0, 0.23, 0.45, and 0.67 wt.% nano-sized Si_3N_4, at loads of 4 N and 8 N and sliding speeds of 0.85 m/s and 1.1 m/s, the following conclusions were drawn:

- Abrasion has been identified as the dominant wear mechanism from worn surface analysis tested at 0.85 and 1.1 m/s of the base alloy and nanocomposites. Adhesion was also identified (Mg-4Zn alloy and Mg-4Zn nanocomposite with 0.67 wt.% Si_3N_4 at 0.85 m/s).
- The addition of Si_3N_4 nanoparticles has not caused too much increase in the density of the Mg-4Zn alloy. This could mean that the products produced from the Mg-4Zn/nano-Si_3N_4 nanocomposites will also be of light weight.
- Grain size of the Mg-4Zn-based materials progressively reduced as the Si_3N_4 wt.% increased from 0 to 0.67 wt.%. The average grain size decreased by 10.6%, 34.62%, and 63.94% with the additions of 0.23, 0.45, and 0.67 wt.% Si_3N_4 to Mg-4Zn. The reduction of the grain size is attributed to the grain-refining effects of the Si_3N_4 wt.% nanoparticles acting as sites for heterogeneous nucleation.
- The addition of 0.23, 0.45, and 0.67 wt.% Si_3N_4 has improved the microhardness by 8.1, 19.5, and 38.67 %. This is due to the various strengthening mechanisms like grain refinement, Orowan strengthening, and load transfer effects brought about by the addition of Si_3N_4 nanoparticles.
- The wear test-based regression model (for prediction) and perturbation plots show that the mass loss (wear) decreases by adding Si_3N_4 nanoparticles as reinforcement to the Mg-4Zn alloy for all the tested conditions. This confirms the hypothesis that the addition of 15-30 nm sized Si_3N_4 nanoparticles to Mg-4Zn alloy to produce nanocomposites has effectively increased the wear properties (reduced the mass loss up to 8.3 % for 0.67 wt.% Si_3N_4 addition) of Mg-4Zn alloy by strengthening/hardening by grain refinement and other mechanisms.

ACKNOWLEDGEMENT

The authors duly acknowledge APJ Abdul Kalam Technological University (APJAKTU), Thiruvananthapuram, Kerala, Center for Engineering Research and Development (CERD), APJAKTU, Thiruvananthapuram, College of Engineering Trivandrum, Nanoshel UK Limited, Intelligent Materials Pvt Ltd, Punjab (for nanomaterials), SwamEquip, Chennai and Mr. Venkat Raghavan of SwamEquip for stir casting, Central Instrumentation Facility (CIF), Indian Institute of Technology (IIT) Palakkad, and its staff, Mr. Mejo A. J, Central Laboratory for Instrumentation and Facilitation (CLIF), University of Kerala, Thiruvananthapuram, Sophisticated Test and Instrumentation Center (STIC India, CUSAT,

Cochin) and its scientist Dr. Shibu M Eappen, Agro Met Lab, Coimbatore and its technical manager, Mr. R. Arunkumar for materials studies, ISRO Inertial Systems Unit (IISU), Thiruvananthapuram, Mr. Joji J Chaman, Mr. Anand P, and ISRO Space Tribology Laboratory (ISTL), IISU, (for wear/tribology and materials studies), technical staff and library staff of IISU, MISA IISU, STAR TOOLS, Thiruvananthapuram for EDM machining, GVPE Corporation, Coimbatore, StatEase Inc., Systech Technocraft Services Pvt. Ltd., Mumbai for Design-Expert software, OriginLab Corporation, Konark Solutions Bangalore Pvt Ltd. for OriginLab and ImageJ for supporting this research.

AUTHOR CONTRIBUTIONS

Anand Natarajan: Conceptualization, Experiments, Theoretical analysis, Writing, Review and Editing.

Ramu Kumar Verma: Experiments, Theoretical analysis, Review and Editing.

Jayprakash Reddy K: Experiments, Theoretical Analysis, Review and editing.

Bijulal D: Supervision, Theoretical Analysis, Review and editing.

Vijayan K: Supervision, Theoretical Analysis, Review and editing.

Prasanth Prabhakaran: Experiments, Theoretical Analysis, Review and editing.

DISCLOSURE STATEMENT

The authors declare that they have no known competing financial interests or personal relationships that could have appeared to influence the work reported in this paper.

ORCID

Anand Natarajan https://orcid.org/0009-0004-3356-9946

Ramu Kumar Verma https://orcid.org/0009-0004-0824-5974

Jayaprakash Reddy K https://orcid.org/0000-0001-6540-141X

Bijulal D https://orcid.org/0000-0003-2712-3097

Vijayan K https://orcid.org/0009-0001-2037-2720

Prasanth Prabhakaran https://orcid.org/0009-0004-0940-595X

REFERENCES

[1] J. Wang, P. Song, S. Huang, and F. Pan, "High-strength and good-ductility Mg–RE–Zn–Mn magnesium alloy with long-period stacking ordered phase," *Mater Lett* 93 (2013) pp. 415–418. https://doi.org/10.1016/J.MATLET.2012.11.076

[2] F. O. Edoziuno, A. A. Adediran, P. O. Emereje, R. O. Akaluzia, and T. C. Jen, "Development of lightweight, creep resistant Mg–Zn–Al alloys for automotive applications: Influence of micro-additions of quaternary elements," *Results in Engineering* 21 (2024) p. 101632. https://doi.org/10.1016/J.RINENG.2023.101632

[3] S. Jaiswal, R. M. Kumar, P. Gupta, M. Kumaraswamy, P. Roy, and D. Lahiri, "Mechanical, corrosion and biocompatibility behaviour of Mg-3Zn-HA biodegradable composites for orthopaedic fixture accessories," *J Mech Behav Biomed Mater* 78 (2018). https://doi.org/10.1016/j.jmbbm.2017.11.030

[4] S. García-Rodríguez, B. Torres, A. Maroto, A. J. López, E. Otero, and J. Rams, "Dry sliding wear behavior of globular AZ91 magnesium alloy and AZ91/SiCp composites," *Wear* 390–391 (2017). https://doi.org/10.1016/j.wear.2017.06.010

[5] A. E. A. Al-maamari, A. A. Iqbal, and D. M. Nuruzzaman, "Wear and mechanical characterization of Mg–Gr self-lubricating composite fabricated by mechanical alloying," *Journal of Magnesium and Alloys* 7 (2) (2019). https://doi.org/10.1016/j.jma.2019.04.002

[6] N. M. Chelliah, H. Singh, and M. K. Surappa, "Correlation between microstructure and wear behavior of AZX915 Mg-alloy reinforced with 12 wt% TiC particles by stir-casting process," *Journal of Magnesium and Alloys* 4 (4) (2016). https://doi.org/10.1016/j.jma.2016.09.002

[7] S. T. Selvamani, S. Premkumar, M. Vigneshwar, P. Hariprasath, and K. Palanikumar, "Influence of carbon nano tubes on mechanical, metallurgical and tribological behavior of magnesium nanocomposites," *Journal of Magnesium and Alloys* 5 (3) (2017). https://doi.org/10.1016/j.jma.2017.08.006

[8] O. , D. O. , K. T. , K. A. , Z. I. , & V. A. Matvienko, " Investigation of Stresses Induced Due to the Mismatch of the Coefficients of Thermal Expansion of the Matrix and the Strengthening Particle in

Aluminum-Based Composites," *Metals (Basel)* 11 (2) (2021) p. 279. https://doi.org/10.3390/met11020279

[9] M. Shen, X. Zhu, B. Han, T. Ying, and J. Jia, "Dry sliding wear behaviour of AZ31 magnesium alloy strengthened by nanoscale SiCp," *Journal of Materials Research and Technology* 16 (2022) pp. 814–823. https://doi.org/10.1016/J.JMRT.2021.12.048

[10] S. J. Huang, A. Abbas, and B. Ballóková, "Effect of CNT on microstructure, dry sliding wear and compressive mechanical properties of AZ61 magnesium alloy," *Journal of Materials Research and Technology* 8 (5) (2019) pp. 4273–4286. https://doi.org/10.1016/J.JMRT.2019.07.037

[11] M. Rashad, F. Pan, M. Asif, J. She, and A. Ullah, "Improved mechanical proprieties of 'magnesium based composites' with titanium-aluminum hybrids," *Journal of Magnesium and Alloys* 3 (1) (2015). https://doi.org/10.1016/j.jma.2014.12.010

[12] S. Zhang *et al.*, "Research on an Mg–Zn alloy as a degradable biomaterial," *Acta Biomater* 6 (2) (2010) pp. 626–640. https://doi.org/10.1016/j.actbio.2009.06.028

[13] J. Wang, Y. Ma, S. Guo, W. Jiang, and Q. Liu, "Effect of Sr on the microstructure and biodegradable behavior of Mg–Zn–Ca-Mn alloys for implant application," *Mater Des* 153 (2018) pp. 308–316. https://doi.org/10.1016/J.MATDES.2018.04.062

[14] B. P. Zhang, Y. Wang, and L. Geng, "Research on Mg-Zn-Ca Alloy as Degradable Biomaterial," in *Biomaterials*, R. Pignatello, Ed., Rijeka: IntechOpen, 2011, ch. 9. https://doi.org/10.5772/23929

[15] D. Wagner, X. Chai, X. Tang, and S. Kou, "Liquation Cracking in Arc and Friction-Stir Welding of Mg-Zn Alloys," *Metallurgical and Materials Transactions A* 46 (2015). https://doi.org/10.1007/s11661-014-2606-5

[16] H. Jia, X. Feng, and Y. Yang, "Influence of solution treatment on microstructure, mechanical and corrosion properties of Mg-4Zn alloy," *Journal of Magnesium and Alloys* 3 (3) (2015). https://doi.org/10.1016/j.jma.2015.08.006

[17] S. Ramesh, G. Anne, H. S. Nayaka, S. Sahu, and M. R. Ramesh, "Investigation of dry sliding wear properties of multi-directional forged Mg–Zn alloys," *Journal of Magnesium and Alloys* 7 (3) (2019). https://doi.org/10.1016/j.jma.2019.05.008

[18] S. Banerjee, S. Poria, G. Sutradhar, and P. Sahoo, "Dry sliding tribological behavior of AZ31-WC nano-composites," *Journal of Magnesium and Alloys* 7 (2) (2019). https://doi.org/10.1016/j.jma.2018.11.005

[19] I. Dinaharan, S. C. Vettivel, M. Balakrishnan, and E. T. Akinlabi, "Influence of processing route on microstructure and wear resistance of fly ash reinforced AZ31 magnesium matrix composites," *Journal of Magnesium and Alloys* 7 (1) (2019). https://doi.org/10.1016/j.jma.2019.01.003

[20] C. Y. H. Lim, D. K. Leo, J. J. S. Ang, and M. Gupta, "Wear of magnesium composites reinforced with nano-sized alumina particulates," in *Wear* (2005). https://doi.org/10.1016/j.wear.2005.02.006

[21] L. Zhang *et al.*, "Tribological Behavior of Carbon Nanotube-Reinforced AZ91D Composites Processed by Cyclic Extrusion and Compression," *Tribol Lett* 66 (2) (2018) p. 71. https://doi.org/10.1007/s11249-018-1018-x

[22] F. L. Riley, "Silicon Nitride and Related Materials," *Journal of the American Ceramic Society* 83 (2) (2000) pp. 245–265. https://doi.org/10.1111/j.1151-2916.2000.tb01182.x

[23] M. Paramsothy, J.Chan, R.Kwok, and M.Gupta, "Enhanced mechanical response of hybrid alloy AZ31/AZ91 based on the addition of Si_3N_4 nanoparticles," *Materials Science and Engineering: A* 528 (21) (2011) pp. 6545-6551. https://doi.org/10.1016/j.msea.2011.05.003

[24] M. B. Pasha, R. C. Sharma, R. N. Rao, S. Ismail, and M. Gupta, "Sliding wear characteristics of Mg/Si3N4 nanocomposites at room and elevated temperatures," *Mater Lett* 329 (2022) p. 133186. https://doi.org/10.1016/J.MATLET.2022.133186

[25] A. Bhadauria, L. K. Singh, and T. Laha, "Effect of physio-chemically functionalized graphene nanoplatelet reinforcement on tensile properties of aluminum nanocomposite synthesized via spark plasma sintering," *J Alloys Compd* 748 (2018) pp. 783–793. https://doi.org/https://doi.org/10.1016/j.jallcom.2018.03.186

[26] J. He *et al.*, "Silicon Nitride Bioceramics Sintered by Microwave Exhibit Excellent Mechanical Properties, Cytocompatibility In Vitro, and Anti-Bacterial Properties," *J Funct Biomater* 14 (11) (2023). https://doi.org/10.3390/jfb14110552

[27] R. Radha and D. Sreekanth, "Mechanical and corrosion behaviour of hydroxyapatite reinforced Mg-Sn alloy composite by squeeze casting for biomedical

applications," *Journal of Magnesium and Alloys* 8 (2) (2020). https://doi.org/10.1016/j.jma.2019.05.010

[28] J. Hashim, L. Looney, and M. S. J. Hashmi, "Metal matrix composites: production by the stir casting method," *J Mater Process Technol* 92–93 (1999) pp. 1–7. https://doi.org/10.1016/S0924-0136(99)00118-1

[29] M. Fellah, M. labaïZ, O. Assala, A. Lost, and L. Dekhil, "Tribological behaviour of AISI 316L stainless steel for biomedical applications," *Tribology - Materials, Surfaces and Interfaces* 7 (2013) pp. 135–149. https://doi.org/10.1179/1751584X13Y.0000000032

[30] N. Parthasarathi, U. Borah, and S. Albert, "Effect of temperature on sliding wear of AISI 316 L(N) stainless steel – Analysis of measured wear and surface roughness of wear tracks," *Mater Des* 51 (2013) pp. 676–682. https://doi.org/10.1016/j.matdes.2013.04.050

[31] S. Y. Zhang and S. S. Feng, "Friction and wear performances of brake material dry sliding against a composite with a semi-interpenetrating network structure of ceramics and Al-alloy," *Tribol Int* 44 (3) (2011) pp. 248–257. https://doi.org/10.1016/j.triboint.2010.10.029

[32] S. Aravindan, P. V. Rao, and K. Ponappa, "Evaluation of physical and mechanical properties of AZ91D/SiC composites by two step stir casting process," *Journal of Magnesium and Alloys* 3 (1) (2015). https://doi.org/10.1016/j.jma.2014.12.008

[33] G. Tosun and M. Kurt, "The porosity, microstructure, and hardness of Al-Mg composites reinforced with micro particle SiC/Al2O3 produced using powder metallurgy," *Compos B Eng* 174 (2019). https://doi.org/0.1016/j.compositesb.2019.106965

[34] W. Jiang, J. Wang, W. Zhao, Q. Liu, D. Jiang, and S. Guo, "Effect of Sn addition on the mechanical properties and bio-corrosion behavior of cytocompatible Mg–4Zn based alloys," *Journal of Magnesium and Alloys* 7 (1) (2019) pp. 15–26. https://doi.org/10.1016/J.JMA.2019.02.002

[35] F. Yang, S. Zhao, Z. Yang, G. Chen, K. Li, and S. Yuan, "Microstructure and high temperature oxidation resistance of mixed long Si3N4 nanowires with wide diameter distribution," *Mater Res Express* 6 (2019). https://doi.org/10.1088/2053-1591/ab51d8

[36] A. Viswanath, H. Dieringa, K. K. Ajith Kumar, U. T. S. Pillai, and B. C. Pai, "Investigation on mechanical properties and creep behavior of stir cast AZ91-SiCp composites," *Journal of Magnesium and Alloys* 3 (1) (2015). https://doi.org/10.1016/j.jma.2015.01.001

[37] J. M. Mistry and P. P. Gohil, "Experimental investigations on wear and friction behaviour of Si3N4p reinforced heat-treated aluminium matrix composites produced using electromagnetic stir casting process," *Compos B Eng* 161 (2019) pp. 190–204. https://doi.org/10.1016/J.COMPOSITESB.2018.10.074

[38] H. R. Zheng, Z. Li, C. You, D. B. Liu, and M. F. Chen, "Effects of MgO modified β-TCP nanoparticles on the microstructure and properties of β-TCP/Mg-Zn-Zr composites," *Bioact Mater* 2 (1) (2017). https://doi.org/10.1016/j.bioactmat.2016.12.004

[39] M. Omidi, A. Khodabandeh, S. Nategh, and M. Khakbiz, "Wear mechanisms maps of CNT reinforced Al6061 nanocomposites treated by cryomilling and mechanical milling," *Tribol Int* 110 (2017). https://doi.org/10.1016/j.triboint.2017.01.033

[40] E. J. Pavlina and C. Vantyne, "Correlation of Yield Strength and Tensile Strength with Hardness for Steels," *J Mater Eng Perform* 17 (2008) pp. 888–893. https://doi.org/10.1007/s11665-008-9225-5

[41] R. Mehra, H. Singh, and S. K. Chaubey, "Evaluating Surface Roughness of Ductile Cast Iron Machined by EDM Using Solid and Hollow Cylindrical Copper Electrodes," *Periodica Polytechnica Mechanical Engineering* 69 (1) (2025) pp. 46–54. https://doi.org/10.3311/PPme.38763

[42] B. Panda, A. D. Vishwanatha, C. A. Niranjan, P. Harisha, K. R. Chandan, and R. Kumar, "Study of microstructure and wear properties of novel aluminium-modified fly ash composite," *IOP Conf Ser Mater Sci Eng* 561 (1) (2019) p. 12005. https://doi.org/10.1088/1757-99X/561/1/012005

[43] K. A. El-Aziz, D. Saber, and H. E.-D. M. Sallam, "Wear and Corrosion Behavior of Al–Si Matrix Composite Reinforced with Alumina," *J Bio Tribocorros* 1 (1) (2015) p. 5. https://doi.org/10.1007/s40735-014-0005-5

[44] I.-Y. Kim, J.-H. Lee, G.-S. Lee, S.-H. Baik, Y.-J. Kim, and Y.-Z. Lee, "Friction and wear characteristics of the carbon nanotube–aluminum composites with different

manufacturing conditions," *Wear* 267 (1) (2009) pp. 593–598. https://doi.org/10.1016/j.wear.2008.12.096

[45] B. Swain, S. Bhuyan, R. Behera, S. Mohapatra, and A. Behera, "Wear: A Serious Problem in Industry," 2020, pp. 1–20. https://doi.org/10.5772/intechopen.94211

[46] A. Abbas, S. J. Huang, B. Ballóková, and K. Sülleiová, "Tribological effects of carbon nanotubes on magnesium alloy AZ31 and analyzing aging effects on CNTs/AZ31 composites fabricated by stir casting process," *Tribology International* 142 (2020) 105982. https://doi.org/10.1016/j.triboint.2019.105982